

Numerical computation of three-dimensional incompressible Navier–Stokes equations in primitive variable form by DQ method

C. Shu^{*,†}, L. Wang and Y. T. Chew

Department of Mechanical Engineering, National University of Singapore, Singapore 119260, Singapore

SUMMARY

In this paper, the global method of differential quadrature (DQ) is applied to solve three-dimensional Navier–Stokes equations in primitive variable form on a non-staggered grid. Two numerical approaches were proposed in this work, which are based on the pressure correction process with DQ discretization. The essence in these approaches is the requirement that the continuity equation must be satisfied on the boundary. Meanwhile, suitable boundary condition for pressure correction equation was recommended. Through a test problem of three-dimensional driven cavity flow, the performance of two approaches was comparatively studied in terms of the accuracy. The numerical results were obtained for Reynolds numbers of 100, 200, 400 and 1000. The present results were compared well with available data in the literature. In this work, the grid-dependence study was done, and the benchmark solutions for the velocity profiles along the vertical and horizontal centrelines were given. Copyright © 2003 John Wiley & Sons, Ltd.

KEY WORDS: PDQ Method; N–S equations; primitive variable form; SIMPLE strategy; three-dimensional flow; lid-driven cavity flow

INTRODUCTION

The differential quadrature (DQ) method was developed by Bellman *et al.* [1] to approximate the derivative of a smooth function. The DQ method is inspired from the integral quadrature. That is, it approximates the derivative at a mesh point by a weighted sum of all the functional values in the whole domain. Obviously, the key to this method is the determination of weighting coefficients. It was found that the computation of the weighting coefficients depends on the approximation of the function. When the function is approximated by a higher order polynomial, Shu and Richards [2] presented some simple algebraic formulations and recurrence relationship to calculate the weighting coefficients of the first- and higher-order derivatives. For simplicity, this case is called the polynomial-based differential quadrature

*Correspondence to: C. Shu, Department of Mechanical Engineering, National University of Singapore, 10 Kent Ridge Crescent, 119260 Singapore, Singapore.

†E-mail: mpeshuc@nus.edu.sg

(PDQ). When the function is approximated by a Fourier series expansion, Shu and Chew [3] also presented some simple algebraic formulations to compute the weighting coefficients of the first- and second-order derivatives. And this case is termed the Fourier expansion-based differential quadrature (FDQ). So far, the DQ-type methods have been widely applied in the computational mechanics. The mathematical fundamentals of the DQ method and its wide application in engineering were well summarized in the book of Shu [4].

The applications of DQ method in fluid mechanics [2–8] so far were limited to solve the two-dimensional incompressible Navier–Stokes (N–S) equations in vorticity–stream function formulation. These applications showed that DQ is a very efficient and robust numerical method. The major advantage of using vorticity–stream function formulation is that, the momentum equations are replaced by a vorticity transport equation which does not contain pressure gradient. Thus, the difficulty related to the velocity–pressure coupling is eliminated. For the case of two-dimensional incompressible flow, instead of solving the N–S equations with three-dependent variables (two velocity components and pressure), only two-dependent variables (stream function and vorticity) are solved in this formulation. Therefore, less computational effort and storage are needed. The pressure field can be obtained from the converged solutions of stream function and vorticity. However, the major disadvantage of this formulation is that it is difficult to be extended to the three-dimensional case by virtue of the definition of stream function. This is a serious limitation for the stream function–vorticity formulation as most practical problems are three-dimensional in nature. Another disadvantage of vorticity-based formulations is that they require to specify the boundary condition for vorticity at a wall, which may not be physically given.

This paper tries to apply the DQ method to solve the three-dimensional incompressible N–S equations. Up to now, a number of solutions of the three-dimensional incompressible N–S equations have been reported. The formulations used in these work include vector stream function–vorticity formulation by Mallinson and de Vahl Davis [9], velocity–vorticity formulation by Dennis *et al.* [10], velocity–potential formulation by Kim and Moin [11] and primitive variable form by Ku *et al.* [12]. Among these formulations, the primitive variable form appears to be the least complex for solving the three-dimensional N–S equations.

However, there are two major difficulties in solving the primitive variable formulation. Firstly, there is evidently no transport or other equation for pressure. The momentum equations and the continuity equation are intricately coupled since the velocity appears in both the momentum and continuity equations but the pressure only appears in the momentum equations. Secondly, satisfying the continuity equation on the boundary is not automatic, and this condition should be enforced.

To remove the difficulties in solving the primitive variable formulation, Patankar and Spalding [13, 14] proposed an iterative process in 1972 to solve the pressure–velocity linkage problem. The proposed process is termed semi-implicit method for pressure-linked equations (SIMPLE). In this algorithm, an estimated pressure field is used to solve the momentum equations. A pressure correction equation, deduced from the continuity equation, is solved to obtain a pressure correction field that is in turn used to update the velocity and pressure fields. The process continues until the velocity and pressure fields are converged. SIMPLE algorithm is usually applied with lower-order finite difference and finite volume discretization [13–16]. Generally, a staggered grid is needed. When the staggered grid is used, the continuity equation can be satisfied automatically on the boundary. However, the use of staggered grid also results in considerable programming effort.

As discussed above, SIMPLE algorithm is an efficient way to solve primitive variable form of incompressible N–S equations, while DQ is a robust discretization scheme that can generate accurate results by using very few mesh points. In this paper, the SIMPLE strategy is combined with the DQ discretization on a non-staggered grid to solve three-dimensional incompressible N–S equations in primitive variable form. It is believed that this combination holds all the advantages of SIMPLE strategy and DQ method. The use of non-staggered grid can greatly simplify the programming effort. However, this combination faces two major difficulties. One difficulty is how to enforce the continuity equation on the boundary. Since DQ discretization is based on a non-staggered grid, the satisfying of continuity equation on the boundary is not automatic when the primitive variable form is used. It is known that the satisfying of continuity equation is very critical to get the true solution. Thus, one should present some ways to enforce the continuity condition on the boundary. Another difficulty is how to properly implement the boundary condition for pressure correction equation.

In order to solve these problems, two numerical approaches are presented in this paper. The key effort is to propose some ways to enforce the continuity equation on the boundary and to suggest the boundary condition for pressure correction equation. The proposed approaches are validated by their application to simulate the three-dimensional lid-driven cavity flows. It was found that for both approaches, accurate numerical results could be obtained by using a few grid points. Also in this paper, the grid-dependence study is done, and the benchmark solutions for the velocity distributions along the vertical and horizontal centrelines are provided for different Reynolds numbers.

DISCRETIZATION OF DERIVATIVES BY PDQ METHOD

The development of PDQ method [2] is based on the analysis of a linear vector space and of higher-order polynomial approximation. It is assumed that a function is sufficiently smooth so that its derivative at any grid point is approximated by a linear weighted sum of all the functional values in the whole computational domain. For example, the first- and second-order derivatives of a function $f(x)$ at a point x_i can be approximated by

$$f'(x_i) = \sum_{j=1}^N w_{i,j}^{(1)} \cdot f(x_j) \quad (1)$$

$$f''(x_i) = \sum_{j=1}^N w_{i,j}^{(2)} \cdot f(x_j) \quad (2)$$

where N is the total number of grid points. The weighting coefficients $w_{i,j}^{(1)}, w_{i,j}^{(2)}$ are computed by PDQ method as

$$w_{i,j}^{(1)} = \frac{M^{(1)}(x_i)}{(x_i - x_j) \cdot M^{(1)}(x_j)} \quad \text{for } j \neq i \quad (3a)$$

$$w_{i,i}^{(1)} = - \sum_{k=1, k \neq i}^N w_{i,k}^{(1)} \quad (3b)$$

$$w_{i,j}^{(2)} = 2 \cdot w_{i,j}^{(1)} \left(w_{i,i}^{(1)} - \frac{1}{x_i - x_j} \right) \quad \text{for } j \neq i \quad (4a)$$

$$w_{i,i}^{(2)} = - \sum_{k=1, k \neq i}^N w_{i,k}^{(2)} \quad (4b)$$

where $M^{(1)}(x_i) = (x - x_1) \cdot (x - x_2) \cdot \dots \cdot (x - x_{i-1}) \cdot (x - x_{i+1}) \cdot \dots \cdot (x - x_N)$. It is indicated that the weighting coefficients can be computed by a recurrence relationship for the second- and higher-order derivatives [2, 4]. It is shown in Reference [4] that PDQ is equivalent to the highest order finite difference scheme. In other words, it has $(N - m)$ th order of accuracy for the m th order derivative when the number of mesh points is N . Although Equations (1)–(4) can be well applied to both uniform and non-uniform grids, it is recommended to use non-uniform grid with mesh points being clustered near the boundary [4]. Previous work [5, 6] showed that PDQ is more efficient than lower-order FD schemes in terms of accuracy and computational effort.

PRIMITIVE VARIABLE FORMULATION AND BOUNDARY CONDITIONS

The three-dimensional lid-driven cavity flow is considered in this study. The physical boundaries are defined as $s_{x-y}: 0 \leq x \leq 1, 0 \leq y \leq 1$, $s_{x-z}: 0 \leq x \leq 1, 0 \leq z \leq 1$, and $s_{y-z}: 0 \leq y \leq 1, 0 \leq z \leq 1$.

The non-dimensional form of three-dimensional, time-dependent, incompressible N–S equations are taken as the governing equations for this study, which can be written as

$$\frac{\partial u}{\partial t} + u \frac{\partial u}{\partial x} + v \frac{\partial u}{\partial y} + w \frac{\partial u}{\partial z} = - \frac{\partial p}{\partial x} + \frac{1}{Re} \nabla^2 u \quad (5)$$

$$\frac{\partial v}{\partial t} + u \frac{\partial v}{\partial x} + v \frac{\partial v}{\partial y} + w \frac{\partial v}{\partial z} = - \frac{\partial p}{\partial y} + \frac{1}{Re} \nabla^2 v \quad (6)$$

$$\frac{\partial w}{\partial t} + u \frac{\partial w}{\partial x} + v \frac{\partial w}{\partial y} + w \frac{\partial w}{\partial z} = - \frac{\partial p}{\partial z} + \frac{1}{Re} \nabla^2 w \quad (7)$$

$$\frac{\partial u}{\partial x} + \frac{\partial v}{\partial y} + \frac{\partial w}{\partial z} = 0 \quad (8)$$

where u, v , and w are the velocity components along x -direction, y -direction and z -direction, respectively, p is the pressure. Re is the Reynolds number. The physical boundary conditions of the problem are specified as

$$u = 0, \quad v = 0, \quad w = 0 \quad \text{on } s_{y-z}, \quad x = 0 \quad \text{and } 1 \quad (9a)$$

$$u = 1, \quad v = 0, \quad w = 0 \quad \text{on } s_{x-z}, \quad y = 1 \quad (9b)$$

$$u = 0, \quad v = 0, \quad w = 0 \quad \text{on } s_{x-z}, \quad y = 0 \quad (9c)$$

$$u = 0, \quad v = 0, \quad w = 0 \quad \text{on } s_{x-y}, \quad z = 0 \quad \text{and } 1 \quad (9d)$$

NUMERICAL ALGORITHMS

Based on the non-staggered grid, two approaches are presented to solve the N-S equations in primitive variable form. For both approaches, the SIMPLE strategy is used to form the basic iterative process to solve Equations (5)–(8) where the spatial derivatives in three directions are discretized by PDQ method. Each approach proposes its own way to enforce the continuity equation on the boundary and to suggest the boundary condition for pressure correction equation.

Basic iterative process

With an initial estimation of pressure field and the velocity field at the time level n , the application of PDQ method to the spatial derivatives and the first-order forward difference scheme to the temporal derivatives of Equations (5)–(7) gives

$$u_{i,j,k}^* = u_{i,j,k}^n + \Delta t \left[A_{i,j,k}^n - \sum_{ll=1}^N w_{i,ll}^{(1)} p_{ll,j,k}^* \right] \tag{10}$$

$$v_{i,j,k}^* = v_{i,j,k}^n + \Delta t \left[B_{i,j,k}^n - \sum_{ll=1}^M \bar{w}_{j,ll}^{(1)} p_{i,ll,k}^* \right] \tag{11}$$

$$w_{i,j,k}^* = w_{i,j,k}^n + \Delta t \left[C_{i,j,k}^n - \sum_{ll=1}^L \hat{w}_{k,ll}^{(1)} p_{i,j,ll}^* \right] \tag{12}$$

where

$$\begin{aligned} A_{i,j,k}^n &= \frac{1}{Re} \left(\sum_{ll=1}^N w_{i,ll}^{(2)} u_{ll,i,k}^n + \sum_{ll=1}^M \bar{w}_{j,ll}^{(2)} u_{i,ll,k}^n + \sum_{ll=1}^L \hat{w}_{k,ll}^{(2)} u_{i,j,ll}^n \right) - u_{i,j,k}^n \sum_{ll=1}^N w_{i,ll}^{(1)} u_{ll,j,k}^n \\ &\quad - v_{i,j,k}^n \sum_{ll=1}^M \bar{w}_{j,ll}^{(1)} u_{i,ll,k}^n - w_{i,j,k}^n \sum_{ll=1}^L \hat{w}_{k,ll}^{(1)} u_{i,j,ll}^n \\ B_{i,j,k}^n &= \frac{1}{Re} \left(\sum_{ll=1}^N w_{i,j}^{(2)} v_{ll,j,k}^n + \sum_{ll=1}^M \bar{w}_{j,ll}^{(2)} v_{i,ll,k}^n + \sum_{ll=1}^L \hat{w}_{k,j}^{(2)} v_{i,j,ll}^n \right) - u_{i,j,k}^n \sum_{ll=1}^N w_{i,ll}^{(1)} v_{ll,j,k}^n \\ &\quad - v_{i,j}^n \sum_{ll=1}^M \bar{w}_{j,ll}^{(1)} v_{i,ll,k}^n - w_{i,j,k}^n \sum_{ll=1}^L \hat{w}_{k,ll}^{(1)} v_{i,j,ll}^n \\ C_{i,j,k}^n &= \frac{1}{Re} \left(\sum_{ll=1}^N w_{i,ll}^{(2)} w_{ll,j,k}^n + \sum_{ll=1}^M \bar{w}_{j,ll}^{(2)} w_{i,ll,k}^n + \sum_{ll=1}^L \hat{w}_{k,ll}^{(2)} w_{i,j,ll}^n \right) - u_{i,j,k}^n \sum_{ll=1}^N w_{i,ll}^{(1)} w_{ll,j,k}^n \\ &\quad - v_{i,j,k}^n \sum_{ll=1}^M \bar{w}_{j,ll}^{(1)} w_{i,ll,k}^n - w_{i,j,k}^n \sum_{ll=1}^L \hat{w}_{k,ll}^{(1)} w_{i,j,ll}^n \end{aligned}$$

where $w_{i,j}^{(1)}, w_{i,j}^{(2)}$ are the weighting coefficients of the first- and second-order derivatives in the x -direction, while $\bar{w}_{i,j}^{(1)}, \bar{w}_{i,j}^{(2)}$ are the weighting coefficients of the first- and second-order

derivatives in the y -direction, and $\hat{w}_{i,j}^{(1)}, \hat{w}_{i,j}^{(2)}$ are the weighting coefficients of the first- and second-order derivatives in the z -direction.

The intermediate velocity field u^*, v^* and w^* at the time level $n+1$, given from Equations (10)–(12), may not satisfy the continuity equation (8). To satisfy Equation (8), a correction is needed for the velocity and pressure fields, that is

$$u^{n+1} = u^* + u' \quad (13a)$$

$$v^{n+1} = v^* + v' \quad (13b)$$

$$w^{n+1} = w^* + w' \quad (13c)$$

$$p^{n+1} = p^* + p' \quad (13d)$$

It is assumed that Equations (5)–(8) are satisfied for the corrected values of $u^{n+1}, v^{n+1}, w^{n+1}$ and p^{n+1} . Thus, using the same manner, we can obtain

$$u_{i,j,k}^{n+1} = u_{i,j,k}^n + \Delta t \left[A_{i,j,k}^n - \sum_{ll=1}^N w_{i,ll}^{(1)} p_{ll,j,k}^{n+1} \right] \quad (14)$$

$$v_{i,j,k}^{n+1} = v_{i,j,k}^n + \Delta t \left[B_{i,j,k}^n - \sum_{ll=1}^M \bar{w}_{j,ll}^{(1)} p_{i,ll,k}^{n+1} \right] \quad (15)$$

$$w_{i,j,k}^{n+1} = w_{i,j,k}^n + \Delta t \left[C_{i,j,k}^n - \sum_{ll=1}^L \hat{w}_{k,ll}^{(1)} p_{i,j,ll}^{n+1} \right] \quad (16)$$

$$\sum_{ll=1}^N w_{i,ll}^{(1)} \cdot u'_{ll,j,k} + \sum_{ll=1}^M \bar{w}_{j,ll}^{(1)} \cdot v'_{i,ll,k} + \sum_{ll=1}^L \hat{w}_{k,ll}^{(1)} \cdot w'_{i,j,ll} = -S_{i,j,k}^* \quad (17)$$

where $S_{i,j,k}^* = \sum_{ll=1}^N w_{i,ll}^{(1)} \cdot u_{ll,j,k}^* + \sum_{ll=1}^M \bar{w}_{j,ll}^{(1)} \cdot v_{i,ll,k}^* + \sum_{ll=1}^L \hat{w}_{k,ll}^{(1)} \cdot w_{i,j,ll}^*$.

Obviously, subtracting Equation (10) from Equation (14) gives

$$u'_{i,j,k} = -\Delta t \sum_{ll=1}^N w_{i,ll}^{(1)} p'_{ll,j,k} \quad (18)$$

and subtracting Equation (11) from Equation (15) and Equation (12) from Equation (16) leads to

$$v'_{i,j,k} = -\Delta t \sum_{ll=1}^M \bar{w}_{j,ll}^{(1)} p'_{i,ll,k} \quad (19)$$

$$w'_{i,j,k} = -\Delta t \sum_{ll=1}^L \hat{w}_{k,ll}^{(1)} p'_{i,j,ll} \quad (20)$$

Note that the velocity correction u', v' and w' on the boundary are always zero during the iteration process. Thus, when Equations (18)–(20) are substituted into Equation (17),

we get

$$\sum_{ll=1}^N W_{i,ll}^{(2)} p'_{ll,j,k} + \sum_{ll=1}^M \bar{W}_{j,ll}^{(2)} p'_{i,ll,k} + \sum_{ll=1}^L \hat{W}_{k,ll}^{(2)} p'_{i,j,ll} = S_{i,j,k}^* / \Delta t \quad (21)$$

where

$$W_{i,ll}^{(2)} = \sum_{k1=2}^{N-1} w_{i,k1}^{(1)} w_{k1,ll}^{(1)}, \quad \bar{W}_{j,ll}^{(2)} = \sum_{k1=2}^{M-1} \bar{w}_{j,k1}^{(1)} \bar{w}_{k1,ll}^{(1)} \quad \text{and} \quad \hat{W}_{k,ll}^{(2)} = \sum_{k1=2}^{N-1} \hat{w}_{k,k1}^{(1)} \hat{w}_{k1,ll}^{(1)}$$

The use of Equations (10)–(13), (18)–(21) forms a basic iterative process. In the beginning, the initial estimation of velocity and pressure fields given. Then from Equations (10)–(12), the intermediate velocity u^*, v^* and w^* are computed. The obtained u^*, v^* and w^* are there with substituted into Equation (21) to solve for the pressure correction p' . From the pressure correction p' , the velocity correction u', v' and w' can be calculated by Equations (18)–(20). Next, by using Equation (13), the improved velocity and pressure fields can be obtained. After that, we need to check the convergence criteria. If the convergence criteria were satisfied, the computation would be stopped. Otherwise, the improved velocity and pressure fields are taken as the new initial estimation and the above process is repeated until the convergence criteria are satisfied.

As mentioned earlier, PDQ discretization is based on the non-staggered grid, so the continuity equation on the boundary is not automatically satisfied in above process. However, the satisfaction of continuity equation on the boundary is critical for our numerical simulation. When this condition is not satisfied, it implies that there are many sources (sinks) on the boundary, through which the mass flux can flow in or flow out. So the physical problems are altered. To avoid this, the continuity equation, that is, Equation (8), must be accurately satisfied on the boundary. During the above iterative process, another concern is the numerical implementation of boundary condition for pressure correction equation since the physical condition for pressure correction does not exist. The following two approaches give different ways to specify the boundary condition for the pressure correction equation, and to guarantee the satisfaction of continuity equation on the boundary.

Approach 1

It is observed from Equation (13) that p^* is the initial estimation of pressure while p' is the pressure correction. If the pressure is given on the boundary for a problem, p^* should always be chosen as the given value. Then for this case, p' should be taken as zero on the boundary. For a general case, the pressure is usually not given on the boundary, but it can be computed from the momentum equations. For the test problem shown above, the pressure on the boundary can be computed from

$$\frac{\partial p}{\partial x} = \frac{1}{Re} \frac{\partial^2 v}{\partial x^2} \quad \text{at } x = 0, 1, \quad 0 < y < 1, \quad 0 < z < 1 \quad (22a)$$

$$\frac{\partial p}{\partial y} = \frac{1}{Re} \frac{\partial^2 v}{\partial y^2} \quad \text{at } y = 0, 1, \quad 0 \leq x \leq 1, \quad 0 \leq z \leq 1 \quad (22b)$$

$$\frac{\partial p}{\partial z} = \frac{1}{Re} \frac{\partial^2 w}{\partial z^2} \quad \text{at } z = 0, 1, \quad 0 \leq x \leq 1, \quad 0 < y < 1 \quad (22c)$$

Using PDQ method to discretize the spatial derivatives in Equation (22), the pressure on the boundary can be calculated by

$$p_{1,j,k} = \frac{1}{AXN} \left[(w_{N,N}^{(1)} D_{1,j,k} - w_{1,N}^{(1)} D_{N,j,k}) + \sum_{ll=2}^{N-1} (w_{N,ll}^{(1)} w_{1,N}^{(1)} - w_{1,ll}^{(1)} w_{N,N}^{(1)}) p_{ll,j,k} \right] \quad (23a)$$

$$p_{N,j,k} = -\frac{1}{AXN} \left[(w_{N,1}^{(1)} D_{1,j,k} - w_{1,1}^{(1)} D_{N,j,k}) + \sum_{ll=2}^{N-1} (w_{N,ll}^{(1)} w_{1,1}^{(1)} - w_{1,ll}^{(1)} w_{N,1}^{(1)}) p_{ll,j,k} \right] \quad (23b)$$

$$p_{i,1,k} = \frac{1}{AYM} \left[(\bar{w}_{M,M}^{(1)} E_{i,1,k} - \bar{w}_{1,M}^{(1)} E_{i,M,k}) + \sum_{ll=2}^{M-1} (\bar{w}_{M,ll}^{(1)} \bar{w}_{1,M}^{(1)} - \bar{w}_{1,ll}^{(1)} \bar{w}_{M,M}^{(1)}) p_{i,ll,k} \right] \quad (23c)$$

$$p_{i,M,k} = -\frac{1}{AYM} \left[(\bar{w}_{M,1}^{(1)} E_{i,1,k} - \bar{w}_{1,1}^{(1)} E_{i,M,k}) + \sum_{ll=2}^{M-1} (\bar{w}_{M,ll}^{(1)} \bar{w}_{1,1}^{(1)} - \bar{w}_{1,ll}^{(1)} \bar{w}_{M,1}^{(1)}) p_{i,ll,k} \right] \quad (23d)$$

$$p_{i,j,1} = \frac{1}{AZL} \left[(\hat{w}_{L,L}^{(1)} F_{i,j,1} - \hat{w}_{1,L}^{(1)} F_{i,j,L}) + \sum_{ll=2}^{L-1} (\hat{w}_{L,ll}^{(1)} \hat{w}_{1,L}^{(1)} - \hat{w}_{1,ll}^{(1)} \hat{w}_{L,L}^{(1)}) p_{i,j,ll} \right] \quad (23e)$$

$$p_{i,j,L} = -\frac{1}{AZL} \left[(\hat{w}_{L,1}^{(1)} F_{i,j,1} - \hat{w}_{1,1}^{(1)} F_{i,j,L}) + \sum_{ll=2}^{L-1} (\hat{w}_{L,ll}^{(1)} \hat{w}_{1,1}^{(1)} - \hat{w}_{1,ll}^{(1)} \hat{w}_{L,1}^{(1)}) p_{i,j,ll} \right] \quad (23f)$$

where

$$AXN = w_{N,N}^{(1)} w_{1,1}^{(1)} - w_{1,N}^{(1)} w_{N,1}^{(1)}, \quad AYM = \bar{w}_{1,1}^{(1)} \bar{w}_{M,M}^{(1)} - \bar{w}_{M,1}^{(1)} \bar{w}_{1,M}^{(1)}, \quad AZL = \hat{w}_{L,L}^{(1)} \hat{w}_{1,1}^{(1)} - \hat{w}_{1,L}^{(1)} \hat{w}_{L,1}^{(1)}$$

$$D_{1,j,k} = \frac{1}{Re} \sum_{ll=1}^N w_{1,ll}^{(2)} u_{ll,j,k}, \quad D_{N,j,k} = \frac{1}{Re} \sum_{ll=1}^N w_{N,ll}^{(2)} u_{ll,j,k}, \quad E_{i,1,k} = \frac{1}{Re} \sum_{ll=1}^M \bar{w}_{1,ll}^{(2)} v_{i,ll,k}$$

$$E_{i,M,k} = \frac{1}{Re} \sum_{ll=1}^M \bar{w}_{M,ll}^{(2)} v_{i,ll,k}, \quad F_{i,j,1} = \frac{1}{Re} \sum_{ll=1}^L \hat{w}_{1,ll}^{(2)} w_{i,j,ll}, \quad F_{i,j,L} = \frac{1}{Re} \sum_{ll=1}^L \hat{w}_{L,ll}^{(2)} w_{i,j,ll}$$

When pressure on the boundary is determined by Equation (23), the pressure correction on the boundary can be specified as $p' = 0$. Then Equation (21) can be solved by SOR method. However, having the proper boundary condition for pressure correction is not sufficient, which may still lead to inaccurate numerical results. To get the accurate solution, one has to enforce the continuity equation on the boundary.

It can be noted that when the continuity equation is satisfied on the boundary, the following Neumann condition for velocity can be derived:

$$\frac{\partial u}{\partial x} = 0 \quad \text{at } x = 0, 1, \quad 0 < y < 1, \quad 0 < z < 1 \quad (24a)$$

$$\frac{\partial v}{\partial y} = 0 \quad \text{at } y = 0, 1, \quad 0 \leq x \leq 1, \quad 0 \leq z \leq 1 \quad (24b)$$

$$\frac{\partial w}{\partial z} = 0 \quad \text{at } z = 0, 1, \quad 0 \leq x \leq 1, \quad 0 < y < 1 \quad (24c)$$

In this approach, Equation (24) is enforced after the improved velocity field is obtained from Equation (13). Equation (9) provides one boundary condition for the velocity at each boundary point. So, when Equation (24) is also applied, there will be two boundary conditions for the velocity. One condition can be considered as the equation for the boundary point itself, and the other condition (derivative condition) is converted to the equation for its neighbouring point. After PDQ discretization of derivatives in Equation (24), the velocity on the boundary and its neighbouring points can be computed by

$$u_{1,j,k} = 0, u_{N,j,k} = 0, u_{i,1,k} = 0, u_{i,M,k} = 1, u_{i,j,1} = 0, u_{i,j,L} = 0 \tag{25a}$$

$$v_{1,j,k} = 0, v_{N,j,k} = 0, v_{i,1,k} = 0, v_{i,M,k} = 0, v_{i,j,1} = 0, v_{i,j,L} = 0 \tag{25b}$$

$$w_{1,j,k} = 0, w_{N,j,k} = 0, w_{i,1,k} = 0, w_{i,M,k} = 0, w_{i,j,1} = 0, w_{i,j,L} = 0 \tag{25c}$$

$$u_{2,j,k} = \frac{1}{w_{1,2}^{(1)}w_{N,N-1}^{(1)} - w_{N,2}^{(1)}w_{1,N-1}^{(1)}} \left[\sum_{ll=3}^{N-2} (w_{N,ll}^{(1)}w_{1,N-1}^{(1)} - w_{1,ll}^{(1)}w_{N,N-1}^{(1)})u_{ll,j,k} \right] \tag{26a}$$

$$u_{N-1,j,k} = \frac{1}{w_{N,2}^{(1)}w_{1,N-1}^{(1)} - w_{1,2}^{(1)}w_{N,N-1}^{(1)}} \left[\sum_{ll=3}^{N-2} (w_{N,ll}^{(1)}w_{1,2}^{(1)} - w_{1,ll}^{(1)}w_{N,2}^{(1)})u_{ll,j,k} \right] \tag{26b}$$

$$v_{i,2,k} = \frac{1}{\bar{w}_{1,2}^{(1)}\bar{w}_{M,M-1}^{(1)} - \bar{w}_{M,2}^{(1)}\bar{w}_{1,M-1}^{(1)}} \left[\sum_{ll=3}^{M-2} (\bar{w}_{M,ll}^{(1)}\bar{w}_{1,M-1}^{(1)} - \bar{w}_{1,ll}^{(1)}\bar{w}_{M,M-1}^{(1)})v_{i,ll,k} \right] \tag{27a}$$

$$v_{i,M-1,k} = \frac{1}{\bar{w}_{M,2}^{(1)}\bar{w}_{1,M-1}^{(1)} - \bar{w}_{1,2}^{(1)}\bar{w}_{M,M-1}^{(1)}} \left[\sum_{ll=3}^{M-2} (\bar{w}_{M,ll}^{(1)}\bar{w}_{1,2}^{(1)} - \bar{w}_{1,ll}^{(1)}\bar{w}_{M,2}^{(1)})v_{i,ll,k} \right] \tag{27b}$$

$$w_{i,j,2} = \frac{1}{\hat{w}_{1,2}^{(1)}\hat{w}_{L,L-1}^{(1)} - \hat{w}_{L,2}^{(1)}\hat{w}_{1,L-1}^{(1)}} \left[\sum_{ll=3}^{L-2} (\hat{w}_{L,ll}^{(1)}\hat{w}_{1,L-1}^{(1)} - \hat{w}_{1,ll}^{(1)}\hat{w}_{L,L-1}^{(1)})w_{i,j,ll} \right] \tag{28a}$$

$$w_{i,j,L-1} = \frac{1}{\hat{w}_{L,2}^{(1)}\hat{w}_{1,L-1}^{(1)} - \hat{w}_{1,2}^{(1)}\hat{w}_{L,L-1}^{(1)}} \left[\sum_{ll=3}^{L-2} (\hat{w}_{L,ll}^{(1)}\hat{w}_{1,2}^{(1)} - \hat{w}_{1,ll}^{(1)}\hat{w}_{L,2}^{(1)})w_{i,j,ll} \right] \tag{28b}$$

It is noted that in this approach, Equation (13d) is only applied to the interior mesh points. Since the pressure on the boundary is directly computed from the momentum equations, the pressure field obtained by this approach is a true field.

Approach 2

In this approach, the satisfying of continuity equation on the boundary and the implementation of boundary condition for pressure correction are combined. In other words, the boundary condition for pressure correction is derived from the continuity equation on the boundary. The idea of this approach is very similar to the one used in the pseudo-spectral method [17].

Substituting Equations (13a)–(13c) into Equation (8), we obtain

$$\frac{\partial u'}{\partial x} = -\frac{\partial u^*}{\partial x} \quad \text{at } x = 0, 1, \quad 0 < y < 1, \quad 0 < z < 1 \tag{29a}$$

$$\frac{\partial v'}{\partial y} = -\frac{\partial v^*}{\partial y} - \frac{\partial u}{\partial x} \quad \text{at } y=0, 1, \quad 0 \leq x \leq 1, \quad 0 \leq z \leq 1 \quad (29b)$$

$$\frac{\partial w'}{\partial z} = -\frac{\partial w^*}{\partial z} \quad \text{at } z=0, 1, \quad 0 \leq x \leq 1, \quad 0 < y < 1 \quad (29c)$$

Using Equation (18) and PDQ discretization for derivatives, Equation (29a) gives the following condition for p' at the boundary of $i=1$ and N .

$$p'_{1,j,k} = \frac{1}{BXN} (W_{N,N}^{(2)} G_{1,j,k} - W_{1,N}^{(2)} G_{N,j,k}) \quad (30a)$$

$$p'_{N,j,k} = -\frac{1}{BXN} (W_{N,1}^{(2)} G_{1,j,k} - W_{1,1}^{(2)} G_{N,j,k}) \quad (30b)$$

Similarly, using Equations (20) and (21) and PDQ discretization respectively, Equations (29b) and (29c) provide

$$p'_{i,1,k} = \frac{1}{BYM} (\bar{W}_{M,M}^{(2)} H_{i,1,k} - \bar{W}_{1,M}^{(2)} H_{i,M,k}) \quad (31a)$$

$$p'_{i,M,k} = -\frac{1}{BYM} (\bar{W}_{M,1}^{(2)} H_{i,1,k} - \bar{W}_{1,1}^{(2)} H_{i,M,k}) \quad (31b)$$

$$p'_{i,j,1} = \frac{1}{BZL} (\hat{W}_{L,L}^{(2)} R_{i,j,1} - \hat{W}_{1,L}^{(2)} R_{i,j,L}) \quad (32a)$$

$$p'_{i,j,L} = -\frac{1}{BZL} (\hat{W}_{L,1}^{(2)} R_{i,j,1} - \hat{W}_{1,1}^{(2)} R_{i,j,L}) \quad (32b)$$

where

$$BXN = W_{N,N}^{(2)} W_{1,1}^{(2)} - W_{1,N}^{(2)} W_{N,1}^{(2)}, \quad BYM = \bar{W}_{1,1}^{(2)} \bar{W}_{M,M}^{(2)} - \bar{W}_{M,1}^{(2)} \bar{W}_{1,M}^{(2)}$$

$$BZL = \hat{W}_{L,L}^{(2)} \hat{W}_{1,1}^{(2)} - \hat{W}_{1,L}^{(2)} \hat{W}_{L,1}^{(2)}$$

$$G_{1,j,k} = \frac{1}{\Delta t} \sum_{ll=1}^N w_{1,ll}^{(1)} u_{ll,j,k}^* - \sum_{ll=2}^{N-1} W_{1,ll}^{(2)} p'_{ll,j,k}, \quad G_{N,j,k} = \frac{1}{\Delta t} \sum_{ll=1}^N w_{N,ll}^{(1)} u_{ll,j,k}^* - \sum_{ll=2}^{N-1} W_{N,ll}^{(2)} p'_{ll,j,k}$$

$$H_{i,1,k} = \frac{1}{\Delta t} \left(\sum_{ll=1}^M \bar{w}_{1,ll}^{(1)} v_{i,ll,k}^* + \sum_{ll=1}^N w_{i,ll}^{(1)} u_{ll,1,k} \right) - \sum_{ll=2}^{M-1} \bar{W}_{1,ll}^{(2)} p'_{i,ll,k}$$

$$H_{i,M,k} = \frac{1}{\Delta t} \left(\sum_{ll=1}^M \bar{w}_{M,ll}^{(1)} v_{i,ll,k}^* + \sum_{ll=1}^N w_{i,ll}^{(1)} u_{ll,M,k} \right) - \sum_{ll=2}^{M-1} \bar{W}_{M,ll}^{(2)} p'_{i,ll,k}$$

$$R_{i,j,1} = \frac{1}{\Delta t} \sum_{ll=1}^L \hat{w}_{1,ll}^{(1)} w_{i,j,ll}^* - \sum_{ll=2}^{L-1} \hat{W}_{1,ll}^{(2)} p'_{i,j,ll}, \quad R_{i,j,L} = \frac{1}{\Delta t} \sum_{ll=1}^L \hat{w}_{L,ll}^{(1)} w_{i,j,ll}^* - \sum_{ll=2}^{L-1} \hat{W}_{L,ll}^{(2)} p'_{i,j,ll}$$

When the pressure correction at all interior points are computed from Equation (22), the pressure correction on the boundary can be updated by using Equations (30)–(32). It was found that this approach is very sensitive to the singularity of velocity u on the edge of lid wall. To eliminate the effect of singularity, the boundary condition for u was adjusted over a few points so that at $x=0, 1$ and $z=0, 1$ of the lid wall, u is taken as 0, and at the adjacent points of the lid wall, u is adjusted to 0.3 instead of 1.0. The small grid spacing near the boundary should make this approach a reasonable approximation to the original problem.

It should be indicated that, in this approach, the continuity equation and Equation (13d) are applied at all points including the boundary points, but the momentum equations are only applied at interior mesh points. The pressure field obtained by this approach is a relative field.

NUMERICAL RESULTS AND DISCUSSION

The driven cavity flow problem is a standard test case to validate new numerical techniques. Three-dimensional solutions of lid-driven cavity flows have been reported by Ku *et al.* [17], Jiang *et al.* [18] and others [19–23]. The numerical results given by Ku *et al.* [17] were obtained by using Chebyshev pseudospectral method to solve incompressible Navier–Stokes equations in primitive variable, and the results of Jiang *et al.* [18] were obtained by using least-square finite element method to solve velocity–pressure–vorticity formulation. The mesh sizes used by Ku *et al.* [17] are $25 \times 25 \times 13$ for $Re = 100, 400$, and $31 \times 31 \times 16$ for $Re = 1000$, while the mesh size used by Jiang *et al.* [18] is $50 \times 52 \times 50$ for $Re = 100, 400, 1000$. In order to validate the proposed approaches for solving the incompressible Navier–Stokes equations in primitive variable form, the three-dimensional lid-driven cavity flow is considered in this study.

In the present work, the attention is focused on applying proposed approaches to simulate the steady-state lid-driven cavity flow. In the study, the unsteady Navier–Stokes equations are used and processed in time until a steady-state resolution is reached. For the convergence criterion, the absolute maximum residual is set to be less than 10^{-4} for momentum equations and 10^{-6} for pressure correction equation. The PDQ method is used to discretize derivatives in three spatial directions. Numerical simulation was conducted for four Reynolds numbers of $Re = 100, 200, 400$ and 1000 using mesh size of $21 \times 21 \times 21, 23 \times 23 \times 23, 25 \times 25 \times 25$ and $31 \times 31 \times 31$, respectively. The initial values for all the variables at the interior points are set to zero. All the computing processes were carried out on Cray J916. The results were compared with those of Ku *et al.* [17] and Jiang *et al.* [18]. The mesh point distribution in three spatial directions is taken the same, and chosen as

$$x_i = \frac{\cos[\pi/(2N)] - \cos[(2i - 1)\pi/(2N)]}{\cos[\pi/(2N)] - \cos[(2N - 1)\pi/(2N)]}, \quad i = 1, 2, \dots, N \quad (33)$$

where N is the number of grid points. The grid-dependence study was first conducted. It was found that when the mesh size is above a certain value, the numerical results by two proposed approaches are independent of mesh size. Tables I–IV show the grid-dependence results of u -velocity on the vertical centreline and v -velocity on the horizontal centreline at Reynolds number of 100. Also included in these tables are the results of Jiang *et al.* [18]. It is noted

Table I. u -velocity distribution along vertical centreline of the cubic driven cavity calculated by Approach 1.

y	u -velocity calculated by different mesh sizes ($Re=100$)										Jiang <i>et al.</i>
	$11 \times 11 \times 11$	$13 \times 13 \times 13$	$15 \times 15 \times 15$	$17 \times 17 \times 17$	$19 \times 19 \times 19$	$21 \times 21 \times 21$	$23 \times 23 \times 23$	$25 \times 25 \times 25$	$25 \times 25 \times 25$	$50 \times 52 \times 50$	
0.0	0.000	0.000	0.000	0.000	0.000	0.000	0.000	0.000	0.000	0.0000	
0.1	-0.079	-0.073	-0.070	-0.069	-0.069	-0.069	-0.068	-0.068	-0.068	—	
0.2	-0.127	-0.125	-0.124	-0.123	-0.122	-0.122	-0.122	-0.122	-0.122	-0.1155	
0.3	-0.162	-0.170	-0.170	-0.170	-0.170	-0.170	-0.170	-0.170	-0.170	—	
0.4	-0.191	-0.203	-0.205	-0.205	-0.205	-0.205	-0.206	-0.206	-0.206	-0.2017	
0.5	-0.200	-0.208	-0.211	-0.211	-0.211	-0.211	-0.212	-0.212	-0.213	—	
0.6	-0.162	-0.171	-0.173	-0.174	-0.174	-0.174	-0.175	-0.175	-0.175	-0.1732	
0.7	-0.081	-0.087	-0.089	-0.089	-0.089	-0.089	-0.090	-0.090	-0.090	—	
0.8	0.055	0.056	0.055	0.056	0.056	0.055	0.054	0.054	0.054	0.0577	
0.9	0.357	0.360	0.364	0.364	0.363	0.363	0.362	0.362	0.362	—	
1.0	1.000	1.000	1.000	1.000	1.000	1.000	1.000	1.000	1.000	1.0000	

Table II. v -velocity distribution along horizontal centreline of the cubic driven cavity calculated by Approach 1.

x	v -velocity calculated by different mesh sizes ($Re=100$)									
	$11 \times 11 \times 11$	$13 \times 13 \times 13$	$15 \times 15 \times 15$	$17 \times 17 \times 17$	$19 \times 19 \times 19$	$21 \times 21 \times 21$	$23 \times 23 \times 23$	$23 \times 23 \times 23$	$25 \times 25 \times 25$	$25 \times 25 \times 25$
0.0	0.000	0.000	0.000	0.000	0.000	0.000	0.000	0.000	0.000	0.000
0.1	0.105	0.115	0.115	0.117	0.118	0.118	0.118	0.119	0.119	0.119
0.2	0.139	0.143	0.147	0.148	0.150	0.150	0.150	0.151	0.151	0.151
0.3	0.123	0.125	0.128	0.130	0.131	0.131	0.131	0.132	0.132	0.132
0.4	0.079	0.081	0.082	0.083	0.083	0.083	0.083	0.084	0.084	0.084
0.5	0.015	0.013	0.013	0.013	0.013	0.013	0.013	0.013	0.013	0.013
0.6	-0.072	-0.076	-0.078	-0.079	-0.080	-0.080	-0.080	-0.080	-0.080	-0.080
0.7	-0.169	-0.176	-0.179	-0.182	-0.184	-0.184	-0.183	-0.184	-0.184	-0.184
0.8	-0.228	-0.237	-0.241	-0.244	-0.247	-0.246	-0.246	-0.247	-0.247	-0.247
0.9	-0.168	-0.176	-0.179	-0.181	-0.183	-0.182	-0.182	-0.182	-0.182	-0.182
1.0	0.000	0.000	0.000	0.000	0.000	0.000	0.000	0.000	0.000	0.000

Table III. u -velocity distribution along vertical centreline of the cubic driven cavity calculated by Approach 2.

y	u -velocity calculated by different mesh sizes ($Re=100$)										Jiang <i>et al.</i>	
	$11 \times 11 \times 11$	$13 \times 13 \times 13$	$15 \times 15 \times 15$	$17 \times 17 \times 17$	$19 \times 19 \times 19$	$21 \times 21 \times 21$	$23 \times 23 \times 23$	$25 \times 25 \times 25$	$50 \times 52 \times 50$			
0.0	0.000	0.000	0.000	0.000	0.000	0.000	0.000	0.000	0.000	0.000	0.0000	
0.1	-0.064	-0.067	-0.067	-0.068	-0.068	-0.068	-0.068	-0.068	-0.068	-0.068	—	
0.2	-0.117	-0.120	-0.120	-0.121	-0.121	-0.121	-0.121	-0.121	-0.121	-0.121	-0.1155	
0.3	-0.161	-0.167	-0.167	-0.169	-0.169	-0.169	-0.170	-0.170	-0.170	-0.170	—	
0.4	-0.194	-0.201	-0.203	-0.204	-0.205	-0.206	-0.206	-0.206	-0.206	-0.206	-0.2017	
0.5	-0.199	-0.208	-0.208	-0.211	-0.211	-0.211	-0.212	-0.212	-0.213	-0.213	—	
0.6	-0.161	-0.169	-0.171	-0.173	-0.174	-0.175	-0.175	-0.175	-0.175	-0.175	-0.1732	
0.7	-0.079	-0.087	-0.086	-0.090	-0.089	-0.090	-0.090	-0.090	-0.090	-0.090	—	
0.8	0.059	0.055	0.055	0.054	0.055	0.054	0.054	0.054	0.054	0.054	0.0577	
0.9	0.364	0.357	0.362	0.362	0.361	0.361	0.362	0.362	0.362	0.362	—	
1.0	1.000	1.000	1.000	1.000	1.000	1.000	1.000	1.000	1.000	1.000	1.0000	

Table IV. v -velocity distribution along horizontal centreline of the cubic driven cavity calculated by Approach 2.

x	v -velocity calculated by different mesh sizes ($Re=100$)											
	$11 \times 11 \times 11$	$13 \times 13 \times 13$	$15 \times 15 \times 15$	$17 \times 17 \times 17$	$19 \times 19 \times 19$	$21 \times 21 \times 21$	$23 \times 23 \times 23$	$25 \times 25 \times 25$				
0.0	0.000	0.000	0.000	0.000	0.000	0.000	0.000	0.000	0.000	0.000	0.000	
0.1	0.112	0.120	0.118	0.120	0.120	0.120	0.120	0.120	0.120	0.120	0.121	
0.2	0.143	0.150	0.151	0.152	0.152	0.152	0.153	0.153	0.153	0.153	0.153	
0.3	0.129	0.131	0.132	0.133	0.133	0.133	0.133	0.133	0.133	0.133	0.133	
0.4	0.085	0.085	0.084	0.085	0.085	0.085	0.085	0.085	0.085	0.085	0.085	
0.5	0.017	0.014	0.014	0.014	0.014	0.013	0.013	0.013	0.013	0.013	0.013	
0.6	-0.075	-0.078	-0.079	-0.080	-0.080	-0.080	-0.081	-0.081	-0.081	-0.081	-0.081	
0.7	-0.179	-0.184	-0.184	-0.185	-0.185	-0.185	-0.186	-0.186	-0.186	-0.186	-0.186	
0.8	-0.244	-0.249	-0.248	-0.249	-0.249	-0.249	-0.249	-0.249	-0.249	-0.249	-0.249	
0.9	-0.184	-0.185	-0.184	-0.184	-0.184	-0.184	-0.184	-0.184	-0.184	-0.184	-0.184	
1.0	0.000	0.000	0.000	0.000	0.000	0.000	0.000	0.000	0.000	0.000	0.000	

Table V. u -velocity distribution along the vertical centreline through geometric centre of 3D cavity.

y	u -velocity calculated at different Reynolds numbers			
	100	200	400	1000
0.00	0.000	0.000	0.000	0.000
0.05	-0.037	-0.050	-0.088	-0.197
0.10	-0.068	-0.093	-0.152	-0.273
0.15	-0.095	-0.130	-0.200	-0.270
0.20	-0.122	-0.163	-0.229	-0.214
0.25	-0.146	-0.190	-0.235	-0.145
0.30	-0.169	-0.209	-0.216	-0.090
0.35	-0.190	-0.216	-0.180	-0.052
0.40	-0.206	-0.211	-0.134	-0.025
0.45	-0.214	-0.192	-0.089	-0.007
0.50	-0.213	-0.162	-0.048	0.008
0.55	-0.200	-0.125	-0.014	0.022
0.60	-0.175	-0.084	0.015	0.035
0.65	-0.139	-0.043	0.039	0.048
0.70	-0.090	-0.003	0.062	0.062
0.75	-0.028	0.037	0.083	0.078
0.80	0.054	0.083	0.106	0.097
0.85	0.174	0.150	0.138	0.120
0.90	0.361	0.284	0.213	0.157
0.95	0.644	0.563	0.455	0.308
1.00	1.000	1.000	1.000	1.000

Table VI. v -velocity distribution along the horizontal centreline through geometric centre of 3D cavity.

x	v -velocity calculated at different Reynolds numbers			
	100	200	400	1000
0.00	0.000	0.000	0.000	0.000
0.05	0.074	0.092	0.139	0.195
0.10	0.120	0.143	0.196	0.245
0.15	0.145	0.163	0.207	0.232
0.20	0.153	0.164	0.197	0.195
0.25	0.147	0.155	0.180	0.158
0.30	0.133	0.140	0.160	0.126
0.35	0.112	0.120	0.138	0.099
0.40	0.085	0.098	0.115	0.077
0.45	0.052	0.071	0.090	0.057
0.50	0.013	0.039	0.063	0.038
0.55	-0.031	0.000	0.031	0.019
0.60	-0.081	-0.049	-0.005	0.000
0.65	-0.134	-0.109	-0.051	-0.020
0.70	-0.186	-0.179	-0.113	-0.043
0.75	-0.228	-0.250	-0.199	-0.077
0.80	-0.249	-0.303	-0.303	-0.143
0.85	-0.236	-0.305	-0.378	-0.278
0.90	-0.184	-0.240	-0.340	-0.429
0.95	-0.099	-0.123	-0.177	-0.309
1.00	0.000	0.000	0.000	0.000

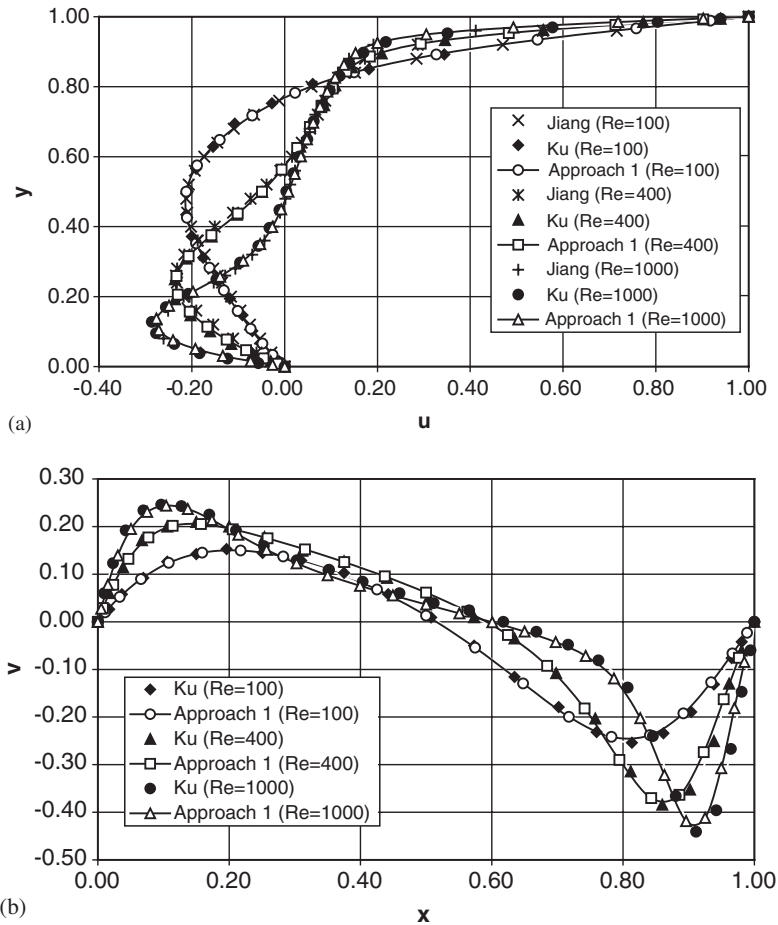


Figure 1. Comparison of velocity distribution calculated by Approach 1 and available data in the literature. (a) Distribution of u -velocity along the vertical centreline of cubic cavity (u - y) and (b) distribution of v -velocity along the horizontal centreline of cubic cavity (x - v).

that the PDQ discretization is based on the non-uniform mesh given by Equation (33). So, the results shown in Tables I-IV were obtained on a uniform mesh by Lagrange interpolation for the sake of comparison. The use of Lagrange interpolation does not affect the accuracy of numerical results since the PDQ method is also based on the Lagrange interpolated polynomial. It can be observed from Tables I-IV that the convergence of numerical results is very good for both approaches. As the number of grid points increases, the accuracy of numerical results is improved very quickly. Meanwhile, it can be seen from these tables that the convergent velocity values by two approaches agree well each other. The present results also agree well with those reported in Reference [18]. Based on the grid-dependence study, we have the ability to give benchmark solutions of the velocity distribution on the vertical centreline and horizontal centreline of 3D driven cavity. The benchmark solutions of velocity profiles along

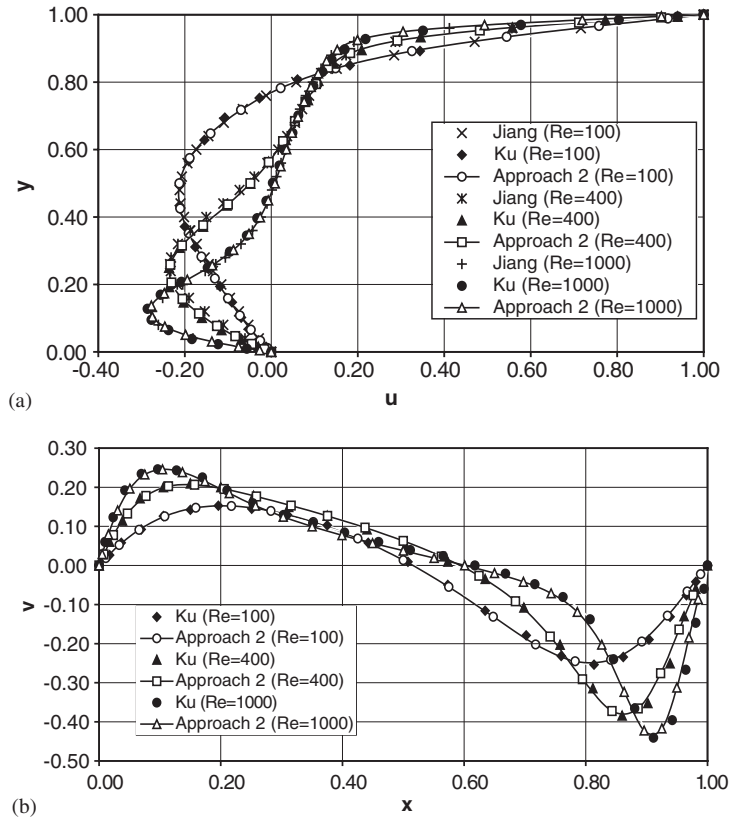


Figure 2. Comparison of velocity distribution calculated by Approach 2 and available data in the literature. (a) Distribution of u -velocity along the vertical centreline of cubic cavity (u - y) and (b) distribution of v -velocity along the horizontal centreline of cubic cavity (x - v).

the vertical and horizontal centrelines for $Re = 100, 200, 400$ and 1000 are given in Tables V and VI. The mesh sizes used for these results are $21 \times 21 \times 21, 23 \times 23 \times 23, 25 \times 25 \times 25$ and $31 \times 31 \times 31$, respectively. It is hoped that the results given in Tables V and VI can be used for comparison by other researchers.

In order to display the numerical results clearly and make the comparison with available data in the literature, the velocity profiles of u component along the vertical centreline and v component along the horizontal centreline on the plane of $z = 0.5$ are plotted in Figures 1 and 2 for $Re = 100, 400$ and 1000 . It can be found that all the velocity profiles by Approaches 1 and 2 agree very well with those of Ku *et al.* [17] and Jiang *et al.* [18].

For details of flow field, Figures 3–5 show the velocity vectors, vorticity and pressure contours computed by Approach 1 on three typical planes for $Re = 100, 400$ and 1000 . For $Re = 100$ and 400 , the flow patterns obtained by Approach 1 agree very well with the results in References [17, 18]. But for $Re = 1000$, the pattern of vorticity contour on the plane $x = 0.5$ has a little deviation from the results in Reference [18].

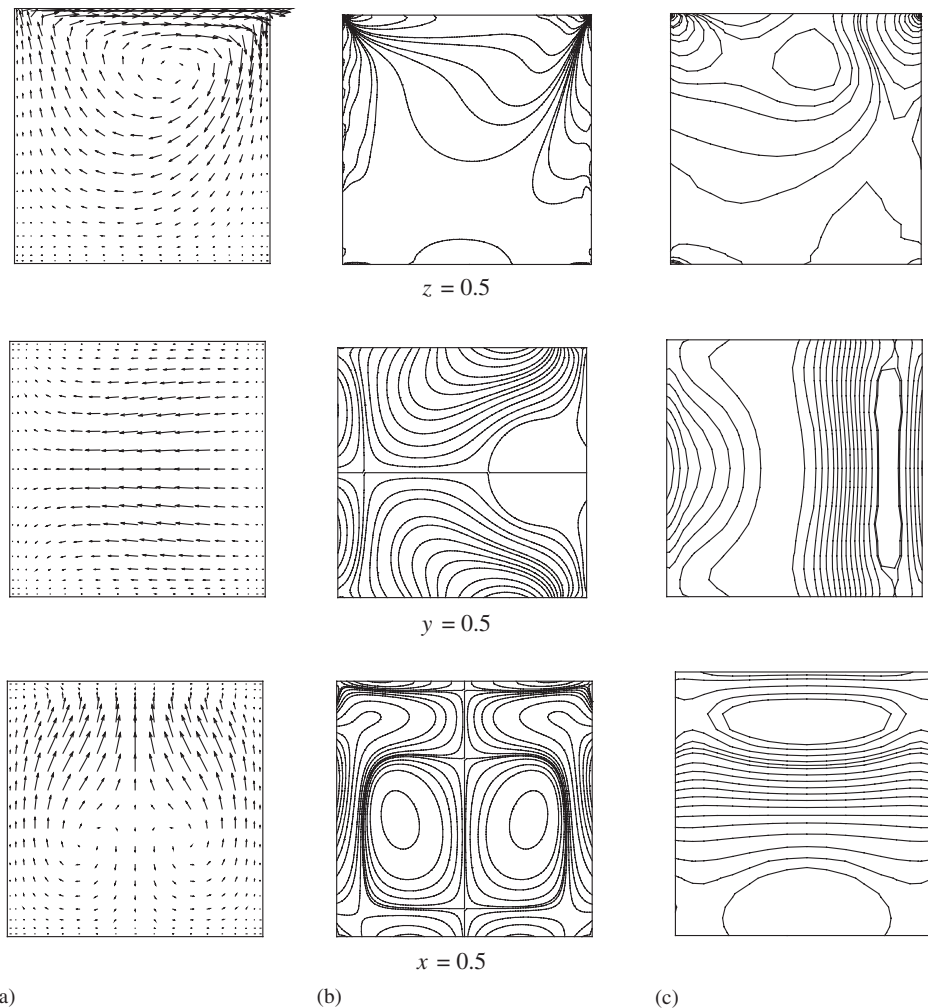


Figure 3. Velocity vectors, vorticity and pressure contours on mid-planes for $Re = 100$ with mesh size of $21 \times 21 \times 21$ by Approach 1. (a) Velocity vectors; (b) vorticity contours and (c) pressure contours.

To make comparison between Approaches 1 and 2, Figures 6–8 display the velocity vectors, vorticity and pressure contours computed by Approach 2 on the same planes for $Re = 100, 400$ and 1000 . For all the cases, the velocity vectors and the vorticity contours agree well with results in References [17, 18] except for the vorticity contour on the plane of $x = 0.5$ at $Re = 1000$. Like the results obtained by Approach 1, the pattern of vorticity contours on the plane of $x = 0.5$ has a little difference with the results in Reference [18]. It can be seen clearly from Figures 3–8 that the patterns of vorticity contours obtained by Approaches 1 and 2 are almost the same for all cases. This fact indicates that our two approaches are consistent. On the other hand, the pressure contours obtained by Approach 2 show some spurious patterns as compared with those obtained by Approach 1. This indicates that the

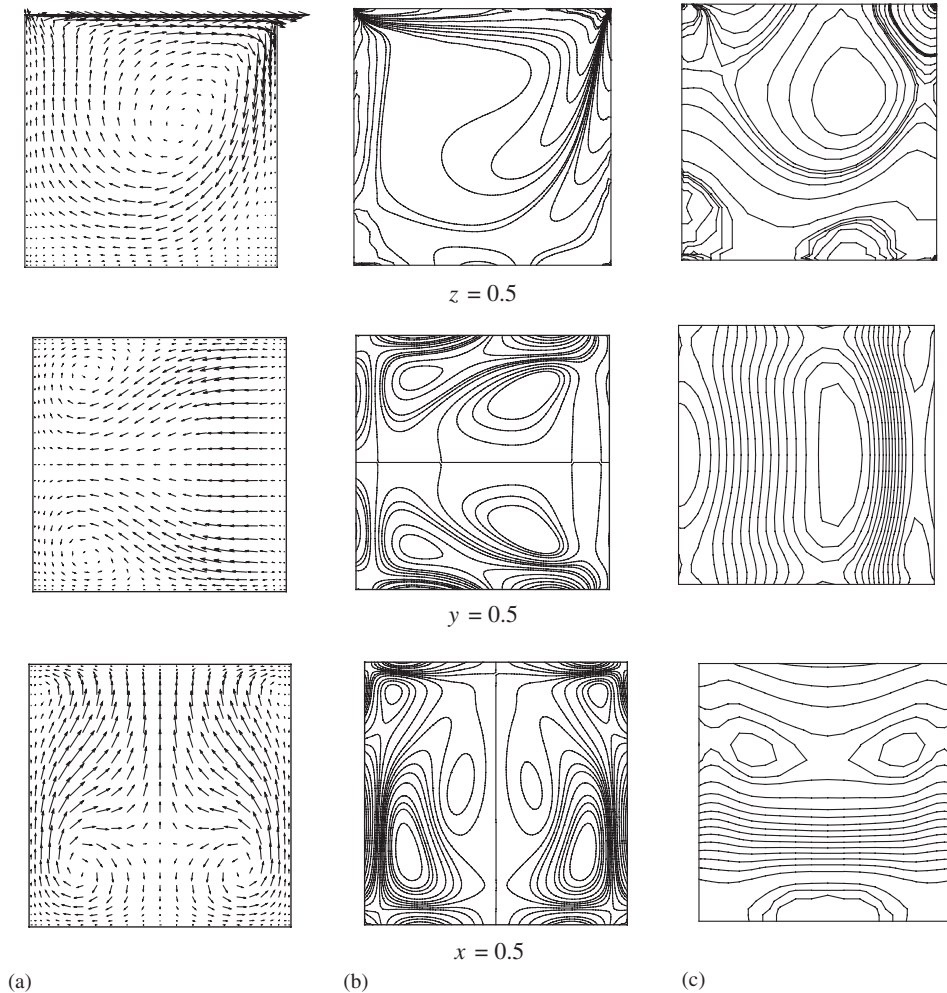


Figure 4. Velocity vectors, vorticity and pressure contours on mid-planes for $Re = 400$ with mesh size of $25 \times 25 \times 25$ by Approach 1. (a) Velocity vectors; (b) vorticity contours and (c) pressure contours.

pressure field obtained by Approach 2 is less accurate than that obtained by Approach 1. In other words, to obtain accurate pressure field, Approach 2 needs more mesh points than Approach 1. To show this, we increase the mesh size from $25 \times 25 \times 25$ to $33 \times 33 \times 25$ and repeat the computation for $Re = 400$. The velocity vectors, vorticity and pressure contours of this computation are shown in Figure 9. It can be seen from Figure 9 that the pressure contours are improved to some extent, but the velocity vectors and the vorticity contours have no obvious change. These results confirm the above analysis on Approach 2, which states that the pressure field is a relative field since the pressure in the whole field including the boundary is updated from the pressure correction. Therefore, the pressure field obtained by Approach 2 cannot represent the true pressure field. From Figure 9, it can be observed that when more

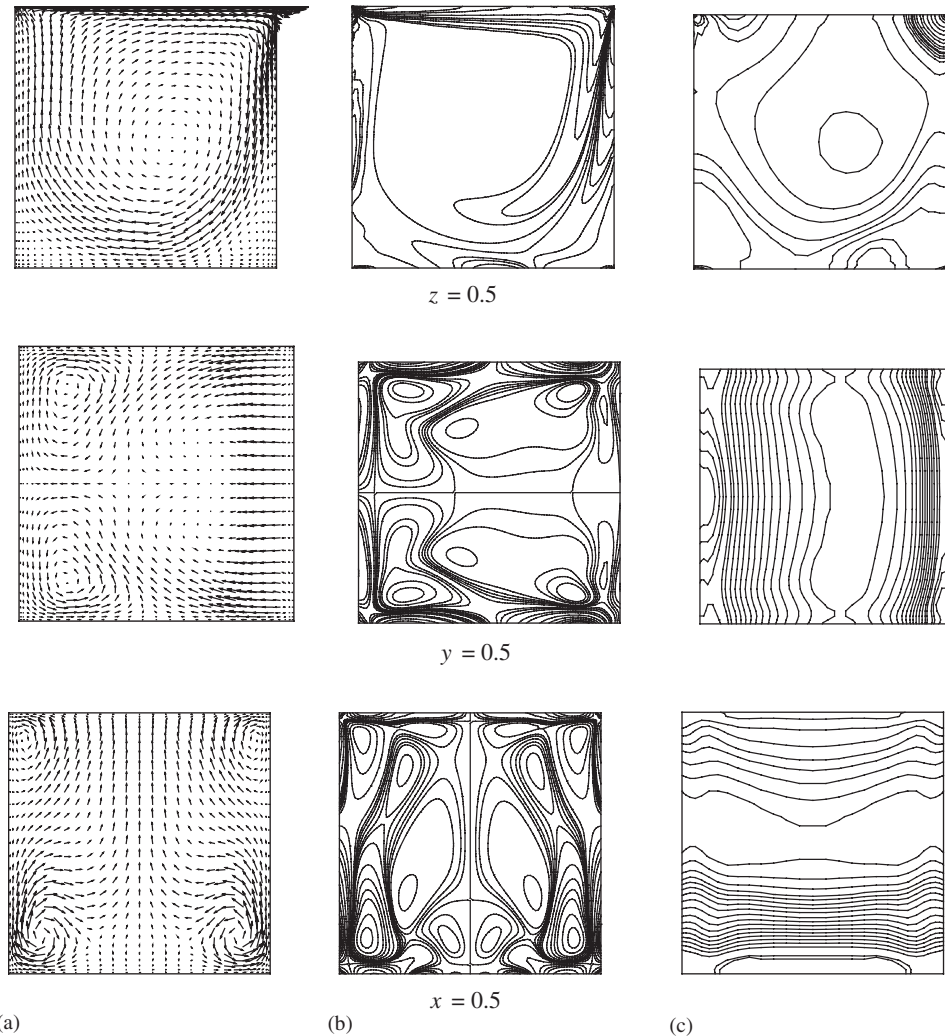


Figure 5. Velocity vectors, vorticity and pressure contours on mid-planes for $Re = 1000$ with mesh size of $31 \times 31 \times 31$ by Approach 1. (a) Velocity vectors; (b) vorticity contours and (c) pressure contours.

mesh points are used to do the calculation, the pressure contours tend to be more accurate, but the pressure contours in the area near the boundary still have some wiggles.

The above results show that the two proposed approaches, which are based on the PDQ discretization on a non-staggered grid, can generally obtain accurate numerical results. However, the two approaches have different features. For Approach 1, the continuity equation on the boundary is enforced in such a way that it is used to compute the velocity at mesh points on the planes of $i = 2$, $i = N - 1$, $j = 2$, $j = M - 1$, and $k = 2$, $k = L - 1$ which are adjacent to the boundary. Therefore, the continuity and momentum equations may not be satisfied

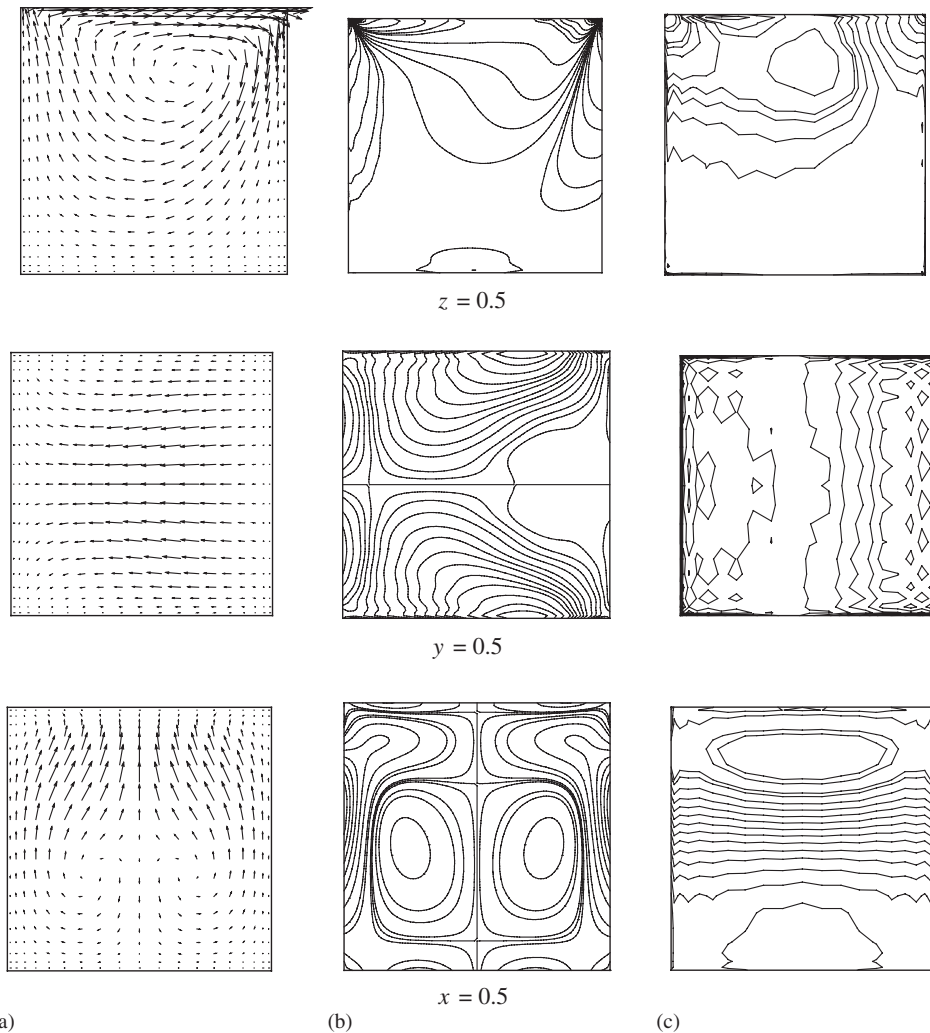


Figure 6. Velocity vectors, vorticity and pressure contours on mid-planes for $Re = 100$ with mesh size of $21 \times 21 \times 21$ by Approach 2. (a) Velocity vectors; (b) vorticity contours and (c) pressure contours.

at these points. By analysing the derivation process of pressure correction equation in Approach 2, it was found that the pressure in the whole field including the boundary is updated from the pressure correction. Therefore, the pressure field is a relative field. From Figure 9, it can be found that much more mesh points are needed by Approach 2 to obtain accurate pressure field as compared with Approach 1. In addition, it was found that Approach 1 is not sensitive to the discontinuity of u -velocity profile on the lid-wall. But for Approach 2, it is needed to smooth the velocity distribution in order to get the reasonable results for vorticity contours. This means that Approach 2 is sensitive to the discontinuity of u -velocity

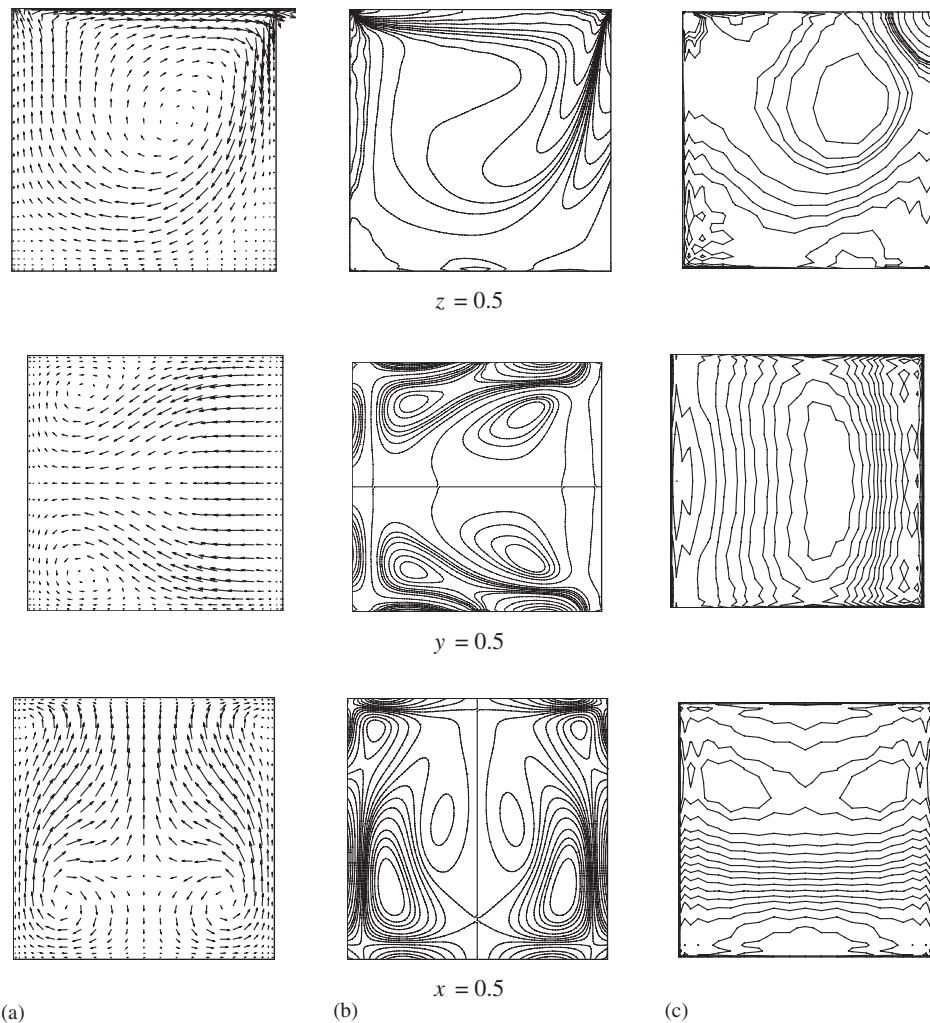


Figure 7. Velocity vectors, vorticity and pressure contours on mid-planes for $Re = 400$ with mesh size of $25 \times 25 \times 25$ by Approach 2. (a) Velocity vectors; (b) vorticity contours and (c) pressure contours.

profile. From this aspect, we think that Approach 1 is more competitive than Approach 2 for solving incompressible Navier–Stokes equations in primitive variable form.

CONCLUSIONS

The three-dimensional Navier–Stokes equations in primitive variable form have been solved successfully by the polynomial-based differential quadrature (PDQ) method for a three-dimensional lid-driven cavity flow. The two approaches, which are based on the PDQ discretization

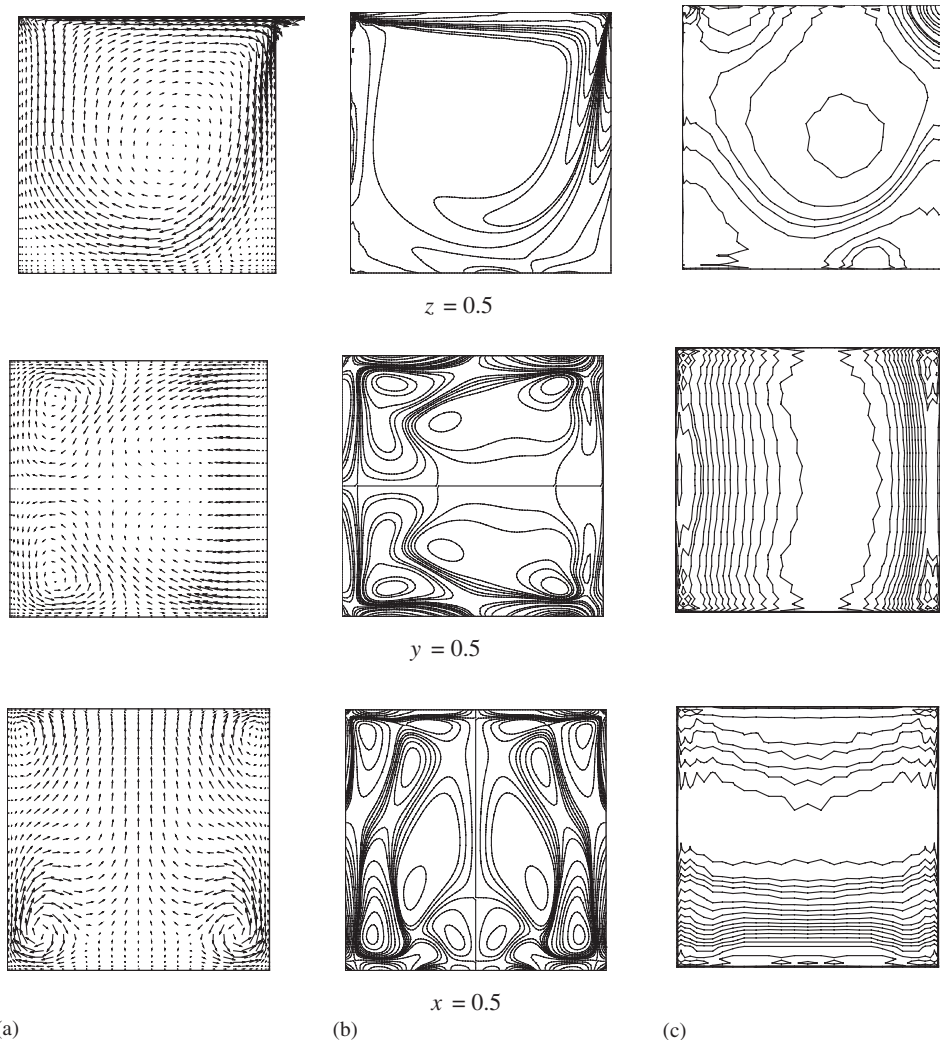


Figure 8. Velocity vectors, vorticity and pressure contours on mid-planes for $Re = 1000$ with mesh size of $31 \times 31 \times 31$ by Approach 2. (a) Velocity vectors; (b) vorticity contours and (c) pressure contours.

on a non-staggered grid and SIMPLE strategy, can obtain accurate numerical results by using a considerably small number of grid points. The steady-state results for the three-dimensional driven cavity flow of $Re = 100, 400$ and 1000 are compared well with available data in the literature. The benchmark solutions of velocity profiles on the vertical centreline and horizontal centreline of 3D cavity are provided in the paper for $Re = 100, 200, 400$ and 1000 . From numerical experiments, it was found that the two approaches yield the same velocity vectors and vorticity distributions. However, Approach 1 gives more accurate pressure field than Approach 2. For all the test cases, we found that the combination of SIMPLE strategy with

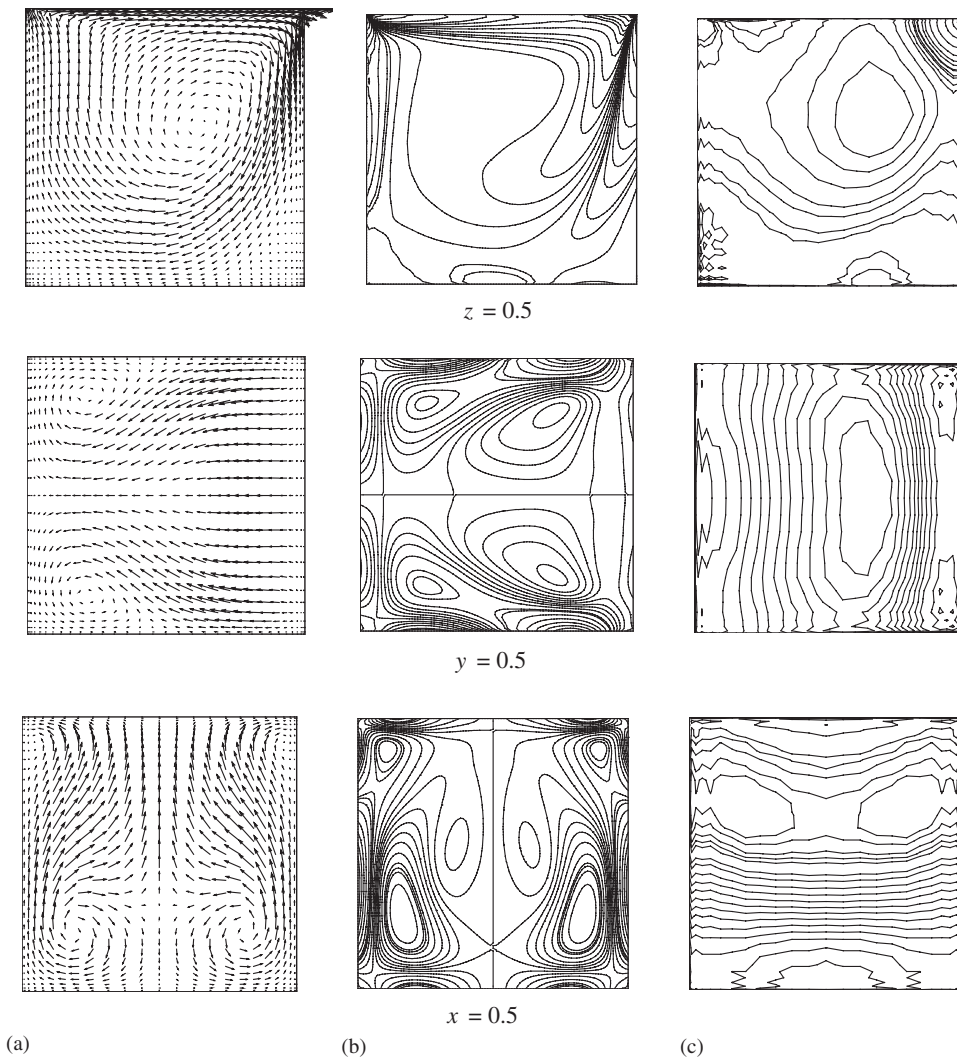


Figure 9. Velocity vectors, vorticity and pressure contours on mid-planes for $Re = 400$ with mesh size of $33 \times 33 \times 25$ by Approach 2. (a) Velocity vectors; (b) vorticity contours and (c) pressure contours.

PDQ discretization is an efficient tool for numerical simulation of three-dimensional incompressible flows.

REFERENCES

1. Bellman RE, Kashef BG, Casti J. Differential quadrature: a technique for the rapid solution of nonlinear partial differential equations. *Journal of Computational Physics* 1972; **10**:40–52.
2. Shu C, Richards BE. Application of generalized differential quadrature to solve two-dimensional incompressible Navier–Stokes equations. *International Journal for Numerical Methods in Fluids* 1992; **15**:791–798.

3. Shu C, Chew YT. Fourier expansion-based differential quadrature and its application to Helmholtz eigenvalue problems. *Communications in Numerical Methods in Engineering* 1997; **13**:643–653.
4. Shu C. *Differential Quadrature and its Application in Engineering*. Springer: London, 2000.
5. Shu C, Yeo KS, Yao Q. On the performance of three iterative methods for solution of GDQ algebraic equations. *Computer Methods in Applied Mechanics and Engineering* 1998; **167**:1–15.
6. Shu C, Wee KHA. Numerical simulation of natural convection in a square cavity by SIMPLE-GDQ method. *Computers & Fluids* 2001; **31**:209–226.
7. Shu C, Khoo BC, Chew YT, Yeo KS. Numerical studies of unsteady boundary layer flows past an impulsively started circular cylinder by GDQ and GIQ approaches. *Computer Methods in Applied Mechanics and Engineering* 1996; **135**:229–241.
8. Shu C. Application of differential quadrature method to simulate natural convection in a concentric annulus. *International Journal for Numerical Methods in Fluids* 1999; **30**:977–993.
9. Mallinson GD, De Vahl Davis G. Three-dimensional natural convection in a box. *Journal of Fluid Mechanics* 1977; **83**:1–31.
10. Dennis SCR, Ingham DB, Cook RN. Finite difference methods for calculating steady incompressible flows in three dimensions. *Journal of Computational Physics* 1979; **33**:325–339.
11. Kim J, Moin P. Application of a fractional-step method to incompressible Navier–Stokes equations. *Journal of Computational Physics* 1985; **59**:308–323.
12. Ku HC, Taylor TD, Hirsh RS. Pseudospectral methods for solution of the incompressible Navier–Stokes equation. *Computers & Fluids* 1987; **15**(2):195–214.
13. Patankar SV, Spalding DB. A calculation procedure for heat and mass transfer in three-dimensional parabolic flows. *International Journal of Heat and Mass Transfer* 1972; **15**:1787–1806.
14. Patankar SV. *Numerical Heat Transfer and Fluid Flow*. McGraw-Hill: New York, 1980.
15. Ghia KN, Sokhey JS. Laminar incompressible viscous flow in curved ducts of rectangular cross-sections. *Journal of Fluids Engineering* 1977; **99**:640–645.
16. Briley WR, McDonald H. Analysis and computation of viscous subsonic primary and secondary flows. *AIAA Paper*, 1979; 79–1453.
17. Ku HC, Hirsh RS, Taylor TD. A pseudospectral method for solution of the three-dimensional incompressible Navier–Stokes equations. *Journal of Computational Physics* 1987; **70**:439–462.
18. Jiang BN, Lin TL, Povinelli LA. Large-scale computation of incompressible viscous flow by least-squares finite element method. *Computer Methods in Applied Mechanics and Engineering* 1994; **114**:213–231.
19. Tang LQ, Cheng T, Tate T, Tsang H. Transient solutions for three-dimensional lid-driven cavity flows by a least-squares finite element method. *International Journal for Numerical Methods in Fluids* 1995; **21**:413–432.
20. Fujima S, Tabata M, Fukasawa Y. Extension to three-dimensional problems of the upwind finite element scheme based on the choice of up- and downwind points. *Computer Methods in Applied Mechanics and Engineering* 1994; **112**:109–131.
21. Ho CJ, Lin FH. Numerical simulation of three-dimensional incompressible flow by a new formulation. *International Journal for Numerical Methods in Fluids* 1996; **23**:1073–1084.
22. Guj G, Stella F. A vorticity–velocity method for the numerical solution of 3D incompressible flows. *Journal of Computational Physics* 1993; **106**:286–298.
23. Guevremont G, Habashi WG, Kotiuga PL. Finite element solution of the 3D compressible Navier–Stokes equations by a velocity–vorticity method. *Journal of Computational Physics* 1993; **107**:176–187.